## Authors' Responses to the comments of Referee #2 on

"Fundamental effect of vibrational mode on vortex-induced vibration in a brimmed diffuser for a wind turbine" by Taeyoung Kim et al. (wes-2020-29)

We are grateful for your valuable comments that help us improve the quality of this manuscript. We replied to your comments as below.

### Comment 1

"Authors decided to focus on 2D simulations, which is reasonable due to the high computational cost of aero-structural simulations, however more specific justification on the technical relevance of this choice is required."

**Response**

This study intends to explain and clarify the fundamental mechanism of the vortex-induced vibration (VIV) in the wind lens structure rather than to perform the realistic simulation of the flow-induced vibration (FIV) of the actual wind lens. In order to obtain a fundamental understanding of the VIV in wind lens and simplify the discussion, we minimized the turbulent effect, 3D wake structure, and the rotor effect in the analysis. On the basis of the reviewer's comment, We plan to add supplementary explanations to the first paragraph on Page 4 in the introduction of the revised manuscript to emphasize the novelty of this paper, including the reason why we reduced our numerical model to the two-dimension and the low Reynolds number, which is written in **Response** to **Comment 5**.

### Comment 2

"Authors make use of a compressible-flow model. Since the Mach number should be well below 0.3, this choice does not seem justified and might even lead to numerical issues if proper preconditioners are not used. Please clarify in the text."

**Response**

According to the literature (Shima, 2015), numerical errors due to the low Mach number increase with decreasing a Mach number less than 0.1 without any preconditioner. In our CFD program, the Mach number was set as 0.1 imaginarily. We confirmed that the calculation results are almost the same with less than 1% error in the Strouhal numbers at the Mach number set as 0.1, 0.2, and 0.3. Our CFD program has been validated in several unsteady aerodynamic studies at low Reynolds number regime. In these studies (Isogai et al, 2004; Yamamoto and Isogai, 2005; Nagai et al, 2009; Nagai and Isogai, 2011; Nagai et al, 2012), the numerical results are in good agreement with the experimental results. In addition, as shown below in **Response** to **Comment 6**, the numerical result is compared to that calculated by using ANSYS CFX with the SST $k$-$\omega$ turbulence model at $Re$ = 288. The vortex shedding frequencies and the vortex intensity in both results are in good agreement.

**Revision**

**Line 190, Page 9:** we plan to add the sentences below at the end of Sect. 3.2.

Additionally, the Mach number in this CFD program was set to 0.1 imaginarily. We confirmed that the calculation results are almost the same with less than 1% error in the Strouhal numbers at Mach numbers of 0.1, 0.2, and 0.3. Also, we compared a numerical result calculated by 2D Reynolds-Averaged Navier-Stokes (RANS) turbulence model simulation with the SST $k$-$\omega$ turbulence model, utilizing the commercial software, ANSYS CFX. The details are discussed in Appendix B. The vortex shedding frequencies and the vortex intensities in both results are

in good agreement.

**References**

Shima, E.: Simple Compressible CFD Solvers' Story, Nagare : Journal of Japan Society of Fluid Mechanics, 34(2), 67-79, 2015 (in Japanese).

Isogai, K., Fujishiro, S., Saitoh, T., Yamamoto, M., Yamasaki, M., and Matsubara, M.: Unsteady Three-Dimensional Viscous Flow Simulation of a Dragonfly Hovering, AIAA J., 42(10), 2053-2059, doi: 10.2514/1.6274, 2004.

Yamamoto, M. and Isogai, K.: Direct Measurement of Unsteady Fluid Dynamic Forces for a Hovering Dragonfly, AIAA J., 43(12), 2475-2480, doi: 10.2514/1.15899, 2005.

Nagai, H., Isogai, K., Fujimoto, T. and Hayase, T.: Experimental and Numerical Study of Forward Flight Aerodynamics of Insect Flapping Wing, AIAA J., 47(3), 730–742, doi:10.2514/1.39462, 2009.

Nagai, H. and Isogai, K.: Effects of Flapping Wing Kinematics on Hovering and Forward Flight Aerodynamics, AIAA J., 49(8), 1750-1762, doi: 10.2514/1.J050968, 2011.

Nagai, H., Isogai, K., Murozono, M. and Fujishiro, T.: INVESTIGATION ON STRUCTURAL AND AERODYNAMIC CHARACTERISTICS OF RESONANT TYPE ELASTIC FLAPPING WING, in 28th Congress of the International Council of the Aeronautical Sciences, p. ICAS 2012-9.5.3, Brisbane, Australia., 2012. http://www.icas.org/ICAS_ARCHIVE/ICAS2012/ABSTRACTS/875.HTM

## Comment 3

"The authors use a deforming mesh strategy to account for the deformation of the structure during motion; some information on the numerical technique used for deforming the mesh should be reported (at least with a citation). Did the Authors experience any issue with cell quality due to mesh deformation during the simulations?"

**Response 1**

The sentence below will be added to the revised version to explain the moving mesh method in **Line 167, Page 7**.

"The moving mesh method based on the geometric conservative law was used (Thomas and Lombard, 1979)."

**Reference to be added**

Thomas, P. D., and Lombard, C. K.: Geometric Conservation Law and Its Application to Flow Computations on Moving Grids, AIAA Journal, 17 (10), 1030–1037, doi: 10.2514/3.61273, 1979.

**Response 2**

In the current manuscript, we mentioned that we could not obtain the convergent results at $U^*$ = 5.1, 5.3, and 5.5 because of the large deformation of the structure occurring in the transient response. Fortunately, we now obtained the limit-cycle oscillation results at $U^*$ = 5.1 and 5.3 by gradually increasing the uniform wind speed, yet we could not obtain a convergent result at $U^*$ = 5.5 because of much larger deformation in the transient response. To present the lock-in more clearly, we plan to replace Figs. 14, 15 and 16 with updated ones, as shown below. In the updated Fig. 16, we arrange the spectrum line of lift and drag at the respective velocities in order to accurately express the discretized data instead of the surface contour of frequency spectra in the whole calculation domain. Even if the figures are updated in the revised version, the explanations related to Figs. 14 and 15 are the same as those in the current manuscript because the tendency of the graphs is the same. Thanks to the updated figures, we add the discussion about the lock-in phenomena in more detail in the revised version.

**Revision**

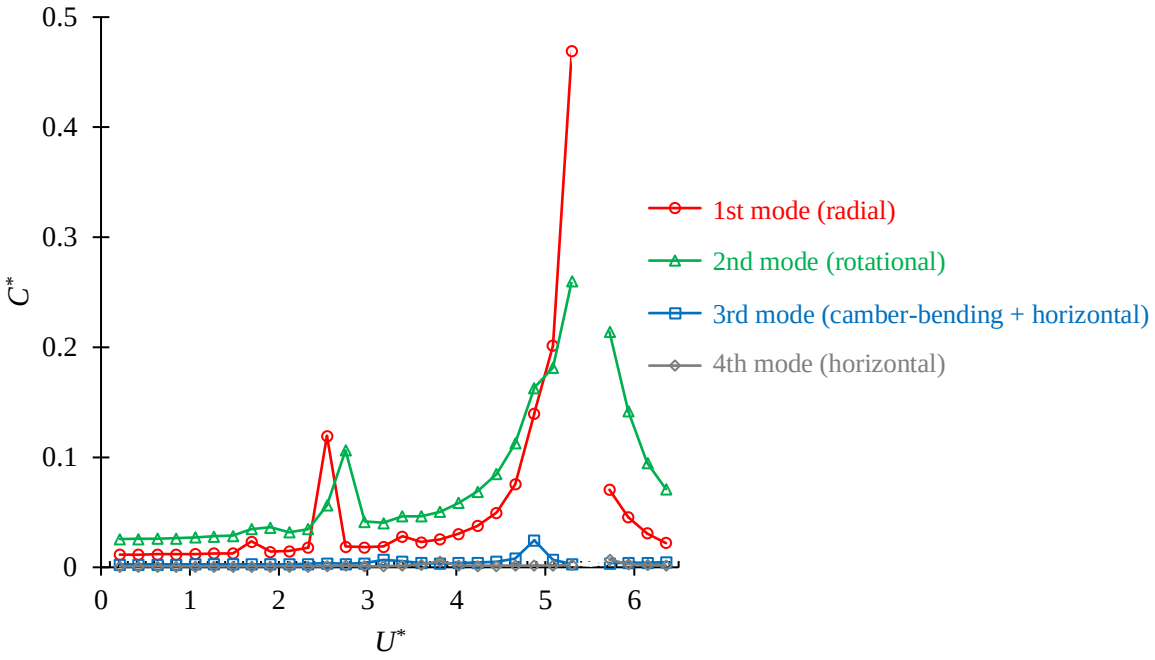


**Figure 14. Compliance of each mode with respect to wind speed in the aeroelastic analysis**

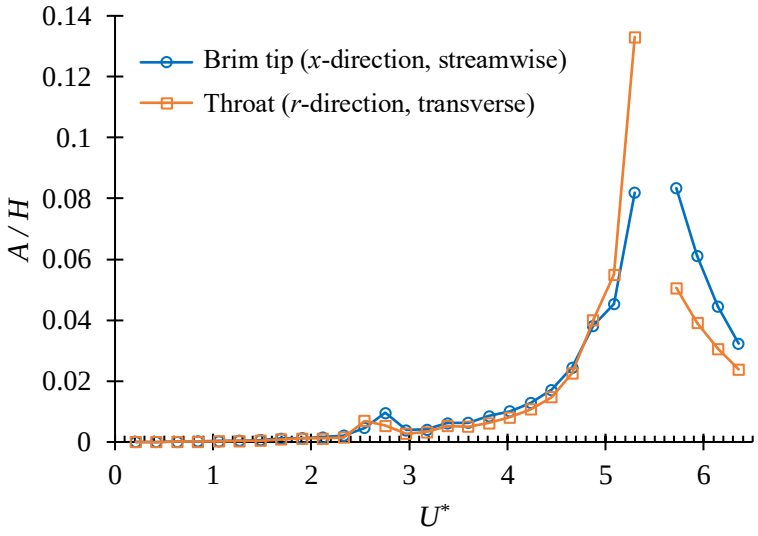


**Figure 15. The displacement amplitude of the brim tip in the x-direction and the throat in the r-direction**

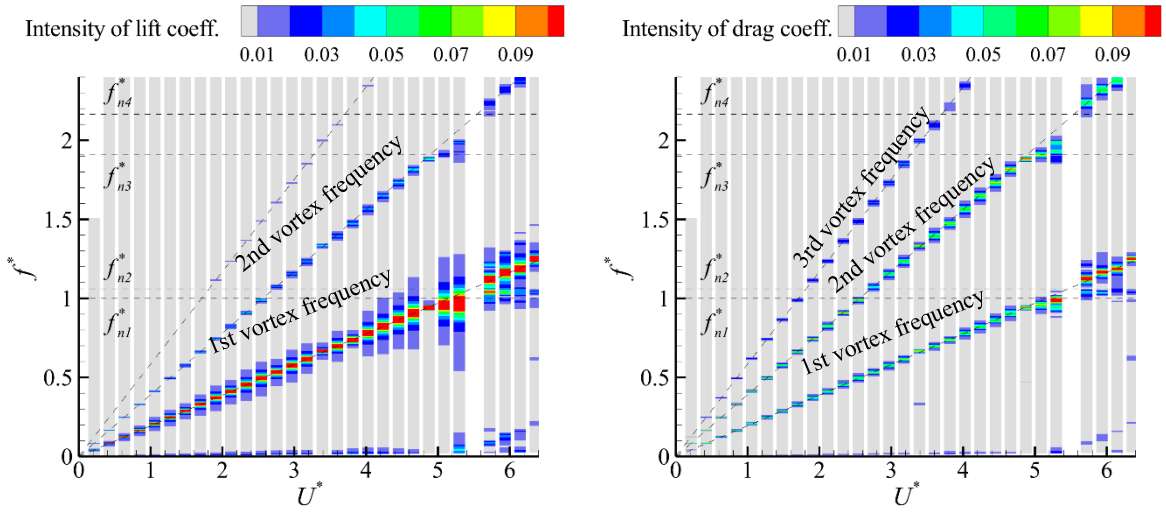


**Figure 16. Frequency spectra of lift and drag at each reduced velocity in the aeroelastic analysis**

**Lines 401–409, Page 19:** The sentence, "The intensities … amplitude vibration", is replaced to the following

The intensities of the lift and drag spectra with respect to the reduced velocity are expressed in Fig. 16. As aforementioned, the result at $U^*$= 5.5, where the computation was aborted due to the excessive deformation in the transient response, is blank. The peak points of the spectra are aligned with the respective straight vortex-shedding frequency lines estimated from the Strouhal numbers in the case where the rigid wind lens section is at rest. However, in the range of $U^*$= 4.9–5.5, the peak points are located along the respective horizontal natural frequency lines, which indicates that a lock-in phenomenon occurs. At $U^*$ = 4.9, the second vortex shedding frequency is captured in the third natural frequency. Nevertheless, the third mode vibration is not excited so much as shown in Fig. 14. At $U^*$ = 5.1 and 5.3, when the first mode vibration is considerably excited as shown in Fig. 14, the first vortex shedding frequency is locked in the first natural frequency. At $U^*$ = 5.5 (blank), the first vortex shedding frequency is likely to match the second natural frequency, which can be inferred from the additional peaks of the lift and drag spectra that appear on the horizontal line of $f^* = f^*_{n2}$ at $U^* \geq 5.7$. On the other hand, there is no noticeable lock-in at $U^*$ = 2.5 and 2.8 at the intersections between the second vortex shedding frequency and the first and second natural frequencies, although the substantial vibration occurs as shown in Fig. 15. According to Kumar et al. (2016), the width in frequency where lock-in occurs is dependent on $A/H$ for a circular cylinder. From Figs. 15 and 16, the difference between lock-in at $U^*$ = 4.9 and non-lock-in at $U^*$ = 2.8 is attributed to $A/H$ = 0.04 and 0.01, respectively.

**References to be added**

Kumar, S., Navrose, and Mittal, S.: Lock-in in forced vibration of a circular cylinder, Phys. Fluids, 28, 113605, doi: 10.1063/1.4967729, 2016.

## Comment 4

"No model of the turbine within the wind lens is considered, at least a comment on this aspect should be reported."

**Response**

The consideration of the rotor is important to a realistic full simulation of VIV for the actual wind lens. However, to minimize the aerodynamic complexity and elicit the fundamental mechanism of VIV for the brimmed diffuser, we removed the rotor from the numerical model. We plan to add the survey of the previous studies about the rotor

effect on the wind lens turbines and the explanation for removing the rotor from our numerical model in the Introduction of the revised manuscript.

The corresponding revision is written in the third paragraph of **Revision** of **Comment 5** below in addition to the other revision of the Introduction.

## Comment 5

"Authors decided to reduce by three orders of magnitude the Reynolds number of the problem, altering the flow regime from turbulent (the actual one) to laminar. Authors state that similarity in aero-elastic response is confirmed despite the alteration of the Reynolds number, but they do not explain how and why. As well known, turbulence is a non-linear phenomenon which does not only feature unsteadiness and instability, but which alters the gross properties of the flow and, hence, the values of lift and drag coefficients, as well as the vortex shedding frequency. Why do the Authors believe that such an arbitrary change in flow regime does not lead to unrealistic results?"

**Response**

As mentioned in **Response** to **Comment 1**, the objective of this study is to reveal the fundamental mechanism of VIV in the wind lens structure with a 2D simplified analytical model. Unintendedly, a lack of explanation and some of words might have led readers to misunderstanding the object of this study. We plan to add supplementary explanations to the Introduction of the revised manuscript to emphasize the novelty of this paper, including the reason why we reduced our numerical model to the two-dimension and the low Reynolds number, as follows.

**Revision**

**The 1st paragraph on Page 4:** The sentence, "Motivated by … numerical simulation", is replaced to the following

Despite many previous studies of VIV for bluff bodies, there is little fundamental understanding of VIV of the brimmed diffuser, whose aerodynamic characteristics contain those of both bluff bodies and airfoils. The brimmed-diffuser section always generates a larger mean lift force with circulation than a mean drag force. On the contrary, the general bluff bodies, such as a circular or rectangular cylinder, generate lift and drag fluctuation, in which the lift force averages zero over time. From this point of view, the aerodynamics of the brimmed-diffuser section resembles that of an airfoil with a large flap angle at a high angle of attack after stall, rather than that of the bluff bodies. Recently, some studies of VIV for a simple airfoil without a flap (Skrzypiński et al., 2014; Benner et al., 2019) have been conducted with the interest of VIV for a wind turbine blade in a standstill condition. Nonetheless, the VIV of an airfoil with a large flap after stall, which is similar to the brimmed-diffuser shape, has not received attention because it does not happen in general operation for aircraft and wind turbines.

Motivated by the VIV observed in the actual wind lens, we numerically investigated the fundamental mechanism of VIV for the brimmed-diffuser shape. Considering the average wind speed on April 3, 2012 and the size of the wind lens, the wind lens turbine was in operation at a Reynolds number of approximately 300,000. The Reynolds number near 300,000 is in the critical Reynolds number regime, where the laminar boundary layer of a bluff body undergoes a turbulent transition, and the wake is disorganized and has 3D vortex structures (Williamson, 1996; Anderson, 2007). Furthermore, the vortex shedding frequency is sensitive to the surface condition of the body and the turbulence intensity of the flow (Zdravkovich, 1990). Because of the complexity of the turbulence and high computational cost, the precise numerical simulation of VIV in the large Reynolds number regime is still challenging even for a circular cylinder (Sarpkaya, 2004; Nguyen and Nguyen, 2016).

Another factor to complicate the flow around the brimmed diffuser is a rotor effect. According to Hasegawa et al. (2007), the rotor inside the wind lens causes a three-dimensional flow around the wind lens, whereas the flow around the wind lens without a rotor tends to be two-dimensional. In addition, the vortex generated by the rotor blade tip induces another vortex in the boundary layer of the inner surface of the wind lens, and the induced vortex suppresses flow separation from the inner surface of the wind lens, which leads to enhancement of collection and

acceleration of the wind (Takahashi et al., 2012). Then, the blade tip vortices and the induced vortices rapidly weaken with their interaction, while the blade tip vortex without the brimmed diffuser remains even in the far downstream region (Abe et al., 2009; Takahashi et al., 2012). Despite these studies about the rotor effect on the WLTs, it has been unremarked how the rotor affects the frequency or intensity of the vortex shedding from the brimmed diffuser.

To initiate the fundamental investigation of VIV for the brimmed-diffuser shape, it is reasonable to simplify the analytical model by minimizing complexities, such as the turbulent effect, 3D wake structure, and the rotor effect. Therefore, the purpose of this paper is not to simulate the observed VIV for the actual wind lens, but rather to clarify the fundamental mechanism of VIV for the brimmed-diffuser shape. To elicit the fundamental mechanism of VIV, the 2D aerodynamic model is employed at a low Reynolds number of 288 with the rotor excluded, where the vortex shedding structures can be treated as 2D in the wake. The vibrational modal characteristics for the whole 3D wind lens are calculated by using the finite element method (FEM). Coupled with the equations of motion in the modal space, 2D unsteady aeroelastic simulation based on 2D Navier-Stokes equations is performed.

**References to be added**

Benner, B. M., Carlson, D. W., Seyed-Aghazadeh, B., and Modarres-Sadeghi, Y.: Vortex-Induced Vibration of Symmetric airfoils used in Vertical-Axis Wind Turbines, Journal of Fluids and Strucutures, 91, 102577, doi: 10.1016/j.jfluidstructs.2019.01.018, 2019.

Hasegawa, M., Ohya, Y. and Kume, H.: Numerical Studies of Flows Around a Wind Turbine Equipped with Flanged-Diffuser Shroud by Using an Actuator-Disc Model, Trans. Japan Soc. Mech. Eng. Ser. B, 73(733), 1860–1867, doi:10.1299/kikaib.73.1860, 2007. (in Japanese)

Skrzypiński, W. R., Gaunaa, M., Sørensen, N., Zahle, F., and Heinz, J.: Self-induced vibration of a DU96-W-180 airfoil in stall, Wind Energy, 17, pp. 641–655, doi: 10.1002/we.1596, 2014.

Takahashi, S., Hata, Y., Ohya, Y., Karasudani, T. and Uchida, T.: Behavior of the blade tip vortices of a wind turbine equipped with a brimmed-diffuser shroud, Energies, 5(12), 5229–5242, doi:10.3390/en5125229, 2012.

## Comment 6

"with present-day CFD technology it is possible to simulate highly turbulent flows with U-RANS, employing suitable turbulence models (such Spalart-Allmaras or k-w SST models)"

**Response**

An additional 2D CFD for the rigid case at $Re$ = 288 was conducted by using ANSYS CFX with a turbulence model of SST $k$-$\omega$ to be compared with the result of our 2D CFD. The vortex shedding frequencies and the vortex intensity in both results are in good agreement.

**Revision**

**Appendix B:** We plan to add this result as Appendix B as below.

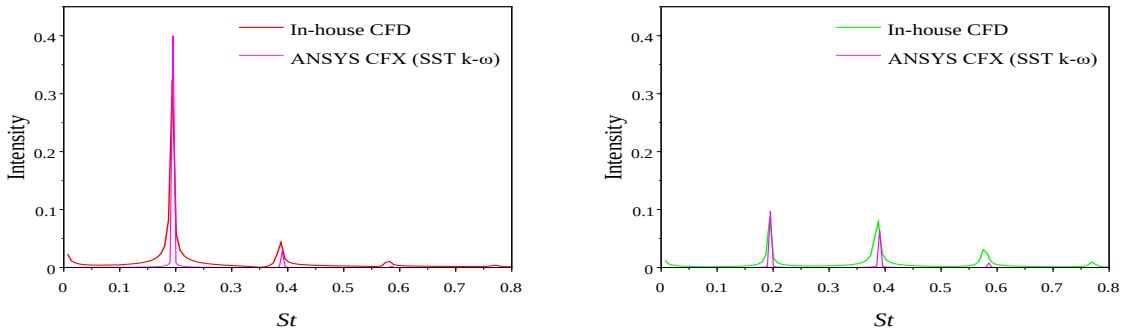


**Figure B 1. Comparison with the frequency spectrum of the lift and drag coefficients calculated by ANSYS CFX with the SST *k-ω* turbulence model**

Appendix B demonstrates a result of the frequency spectrum from the time history of the lift and drag coefficients calculated at $Re$ = 288 by 2D RANS turbulence model simulation, using ANSYS CFX 19.2, to verify that the Strouhal numbers calculated the in-house CFD program are valid. In this case, the SST $k$–$\omega$ turbulence model was applied. The shape and boundary of the computation domain was the same as those in the in-house CFD shown in Fig. 4a, and its domain size was $27.2L \times 13.6L$. The wind lens section is placed where its throat is $0.5D_{\text{thr}}$ above the bottom of the domain and $4.5L$ horizontally away from the left side of the domain. The total number of nodes was 490,142 and the number of elements was 244,175. The time step was 0.001 and the value of $y^+$ was approximately 1. The calculation was conducted until the 70th cycle of the first vortex frequency. Figure B1 shows the frequency spectra of lift and drag calculated by the two different CFD solvers. The two results show a good agreement in the Strouhal numbers although there is a slight difference in the intensity of the respective peaks.